Electric Power Systems Research 199 (2021) 107374

Contents lists available at ScienceDirect

Electric Power Systems Research

journal homepage: www.elsevier.com/locate/epsr

Modeling and control of a hydrogen-based green data center

Nouhaila Lazaar [a,b,*], Mahmoud Barakat [a], Morad Hafiane [b], Jalal Sabor [b], Hamid Gualous [a]

[a] Department of Electrical Engineering, LUSAC Laboratory, University of Caen Normandy, 145 Chemin de la Crespinière, 50130, Cherbourg, France
[b] ENSAM, LSMI Laboratory, University of Moulay Ismail, Marjane 2, 50050, Meknes, Morocco

ARTICLE INFO

Keywords:
Data centers
Energy management
Modeling
Renewable energies
Tidal energy

ABSTRACT

Data centers consume a large amount of energy, contributing to CO_2 emissions, global warming, and resulting in significant electricity cost. To address these concerns, an increasing number of companies have considered building green data centers. The most abundant energy resource is solar; it is now a key player in the global energy transformation. Tidal energy has also received particular attention recently. The predictable characteristic of the resource makes the kinetic energy of tidal current an extremely competitive power resource compared to other commonly used renewable energies. For this purpose, a hybrid Tidal/Photovoltaic system is used for powering an MW scale green data center on a remote island. Green data centers are mainly dependent on renewable energies, which have intermittent nature and require a storage system capable of ensuring sustainable energy feeding. The proposed system consists of an MW scale proton exchange membrane electrolyzer and fuel cell. This system is associated with the $LiFePO_4$ battery to cover the fast-electrical dynamics. In this paper, the system modeling is presented along with an initial proposal of control and energy management system to align the data center energy consumption with the renewable energy generated while respecting the different system constraints. The model is implemented in Matlab/Simulink platform where the simulation results exhibit the system performance under different operation conditions.

1. Introduction

Data centers are facilities composed of servers hosting several types of Information Technology services (IT-services) through an internal network or via internet access [1]. The demand growth for digital services and computing capacity is prompting companies to move to cloud computing. This makes them greedy for electricity consumption, increasing the harmful environmental impact and the associated operational costs. According to [2,3], their total consumption will be between 3% and 13%, best and worst cases respectively of the global electricity production by 2030. Therefore, it is necessary to move towards a renewable energy-based solution to deal with such a considerable challenge. Many IT companies have announced plans to implement green data centers, i.e., data centers partially or entirely powered by renewable energies [4]. These data centers can either use on-site generation options or purchase electricity from the nearest renewable energy plant. For example, Google has purchased 20 years of wind energy from the Iowa Wind Farm to power its data centers in Oklahoma [5]. Facebook has contracted to purchase over 4.0 gigawatts of solar and wind energy to supply their facilities with 100% renewable energy in 2020 [6]. Microsoft has plunged a 450 kW data center into the sea off Orkney to take advantage of tidal energy. The project called "Natick" has been deployed at the European Marine Energy centre (EMEC) [7].

However, reliability and performance are major challenges for data centers when it comes to implementing green computing to meet consumers' needs. Many studies have considered these issues [4,8,9]. In [4], Goiri et al. have designed Parasol, a prototype of a data center powered by green energy that is dedicated to managing the energy demand of workloads, several energy sources (solar and grid), and batteries. The grid was used as a storage device in which the excess energy is saved for later use (Net Metering). Batteries were only discharged when a power failure occurs. The authors have defined a system for planning workload execution and selecting the renewable source to be used, taking into account renewable energy availability, energy demand, and grid energy prices. Recent work in [2] has developed an approach to managing a small data center powered by photovoltaic (PV) panels and connected to the grid. Grange et al. have considered two separate management systems, the first and most relevant to the considered case study is the electrical infrastructure management (energy sources, energy storage, and energy distribution elements). It aims to maximize the use of

* Corresponding author at: 145 Chemin de la Crespinière, 50130 Cherbourg, France.
E-mail address: nouhaila.lazaar@unicaen.fr (N. Lazaar).

https://doi.org/10.1016/j.epsr.2021.107374
Received 23 July 2020; Received in revised form 6 April 2021; Accepted 12 May 2021
Available online 2 June 2021
0378-7796/

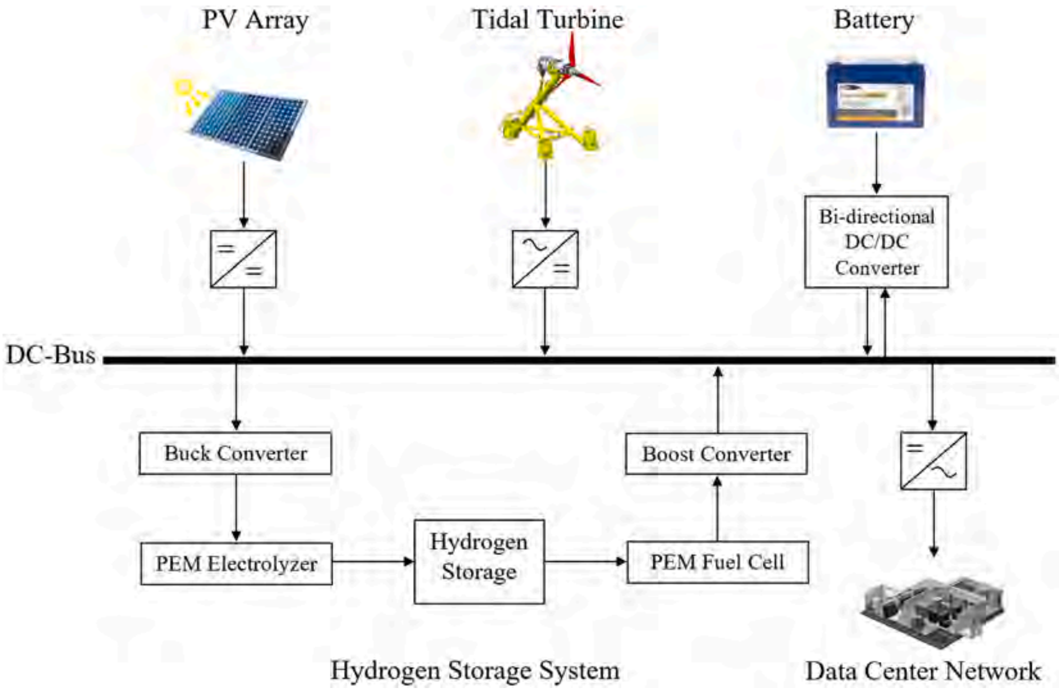

Fig. 1. Hybrid system architecture.

available renewable energies when providing a certain amount of electricity.

Although the above research has considered the energy management in data centers powered by renewable sources, it focused on IT-load scheduling and did not include the modeling of the different electrical subsystems of the microgrid. Besides, the considered data centers are connected to the grid and are based on a single source. Island microgrids can be cost-effective for data centers and provide better power quality in remote areas where the power transmission via cables is either expensive or unfeasible. Furthermore, data centers would not be subject to fluctuations in utility prices and outages which may occur due to disruptive events such as under or over voltage [10]. Due to the intermittent nature of renewable energy, hybrid power systems are proven to be an effective solution for ensuring the reliability of the power supply electricity in remote areas [11]. Wind and solar are the most mature technologies contributing to the electrical energy generation through their integration in a microgrid [12-14]. In 2017, renewable energy capacity in the world had attained 2180 GW, including 390 GW from solar power and 500 GW from wind power [15]. Oceans are recognized as a promising renewable resource for power generation, they cover more than 70% of the earth [16-18]. The energy produced has several forms, encompassing tidal energy, wave energy, thermal, and osmotic energy. Tidal energy is significantly more attractive given the predictability of currents facilitating the management and marketing of the electricity produced, despite the resource intermittency. In France, it is recognized as an electricity production sector that can make an important contribution to the future energy mix [19]. Marine currents of Brittany and Normandy provide a high energy potential. French potential production is estimated to be in the range of 5 to 14 TWh/year [20]. This technology is based on the kinetic energy exploitation of tidal currents according to the same principle as wind turbines. Since water is much denser than air, tidal turbines can capture more energy for a small area with a high level of predictive accuracy (98%) [17,19]. Unlike France, Morocco has not set up yet a center dedicated to tidal energy exploitation. However, the large seas of the Atlantic and the Mediterranean remain an opportunity to develop this technology [21]. Since the kingdom is a country with a high level of sunlight, it has considered solar energy production as a vehicle for modernizing its energy mix [22,23]. Following the success of the solar power plant Noor Ouarzazate with a total capacity of 580 MW, Morocco plans to build Noor Midelt with 825 MW of solar energy by 2022, split between 300 MW of concentrated solar power (CSP) and 525 MW of photovoltaic energy [24].

As a result, our study is focusing on a Tidal/PV hybrid system to power an MW scale data center on a remote island. The combination of solar and tidal power offers a trade-off between the investment costs and space requirements associated with the green data center building, and also help to alleviate the storage system costs. The tidal system consists of a fixed pitch tidal turbine directly coupled to a permanent magnet synchronous generator (PMSG) and connected to a DC link capacitor via a controlled rectifier. Thus, eliminating a significant part of the problems associated with the gearbox use and the pitch angle mechanism. The energy produced from solar panels and tidal turbines suffers from daily, monthly and seasonal variations that are called intermittency. Therefore, an energy storage system must be carefully chosen to ensure the continuous supply of electricity to the data center. The hydrogen system might be one of the best candidates to address the reliability issue [25]. Hydrogen could be renewable based on the source and has clean combustion. Unlike fossil fuels that emit greenhouse gasses, hydrogen combustion does not form Sulphur or carbon derivatives, making it a clean fuel [26]. Furthermore, it has a high heating value per unit of mass [27]. The proposed system is based on a tandem fuel cell/electrolyzer combined with battery storage to cover the fast dynamics of the system.

The main objective of the article is the modeling and simulation while the system sizing and energy management system (EMS) optimization are the scopes of other publications [28,29]. The paper is structured as follows. The modeling of the load, the tidal turbine, the solar panel, the hydrogen storage system, and the battery stack is detailed in Section 2. Section 3 presents the control and energy management strategies used to balance the data center's power consumption with energy production. Simulation results related to the considered case study are discussed in Section 4. Finally, in Section 5, the conclusion and future work are presented.

2. System modeling

To minimize the operating cost and environmental footprint of the

Table 1
Classifications of data centers scale by IT-load.

Size metric	IT-load
Mini	<10 kW
Small	10–150 kW
Medium	150–750 kW
Large	750–2.5 MW
Mega	> 2.5 MW

data center, a hybrid green power generation system is selected to maintain high reliability without an outage. Fig. 1 presents the architecture of the proposed data center powered by several energy sources and storage systems. All energy sources are connected to a common DC bus via power converters. Compared to the AC microgrids, DC microgrids are simpler as they are not concerned with reactive power compensation, frequency stability, and synchronization issues [30].

Modeling is an important step in properly assessing the performance of the hybrid system. The following subsections present the modeling of the proposed microgrid subsystems.

2.1. Load model

Multiple studies have been conducted to model the energy consumption of data centers. Cheung et al. [31] focused on three main energy consumers:

- Servers that are the computers executing the client's requests;
- network equipment that establishes the communication internally between the servers and the communication with the external network;
- power distribution equipment that maintains and delivers electricity to the IT equipment.

This model requires only data from the data center design and its IT equipment specifications. The global model generated is the sum of the equations modeling each part of the data center as shown in (1) [31].

$$P_{IT,dc} = P_{server,\ dc} + P_{network,\ dc} + P_{dist,dc} \tag{1}$$

Data center scale can be defined by the number of servers, the

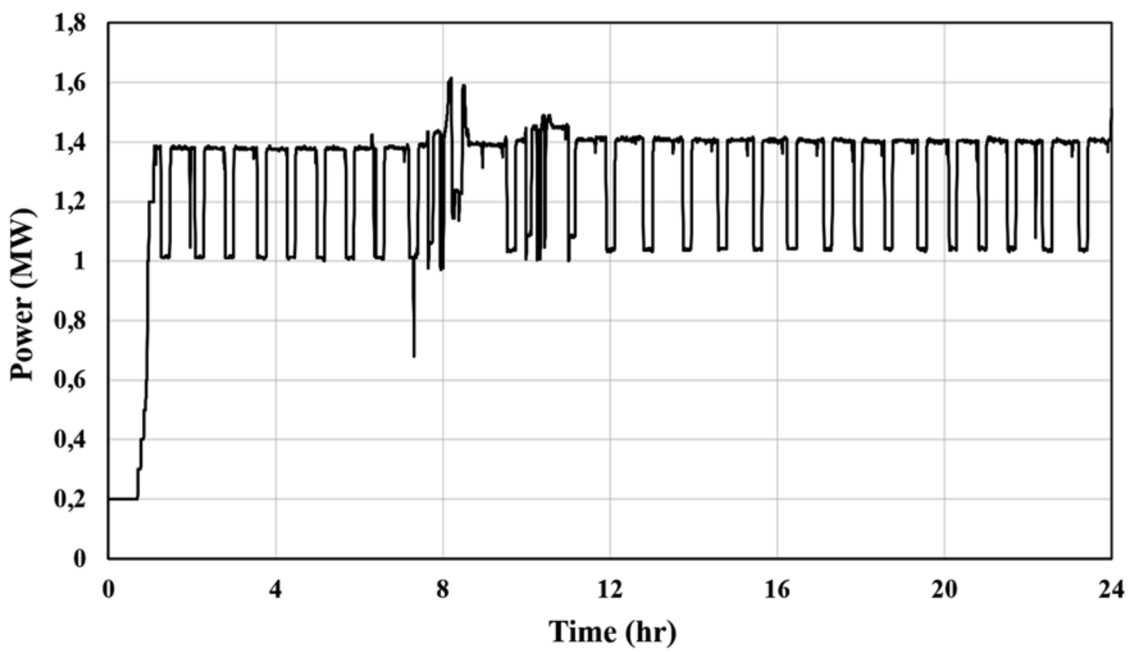

Fig. 2. Data center power consumption during one day.

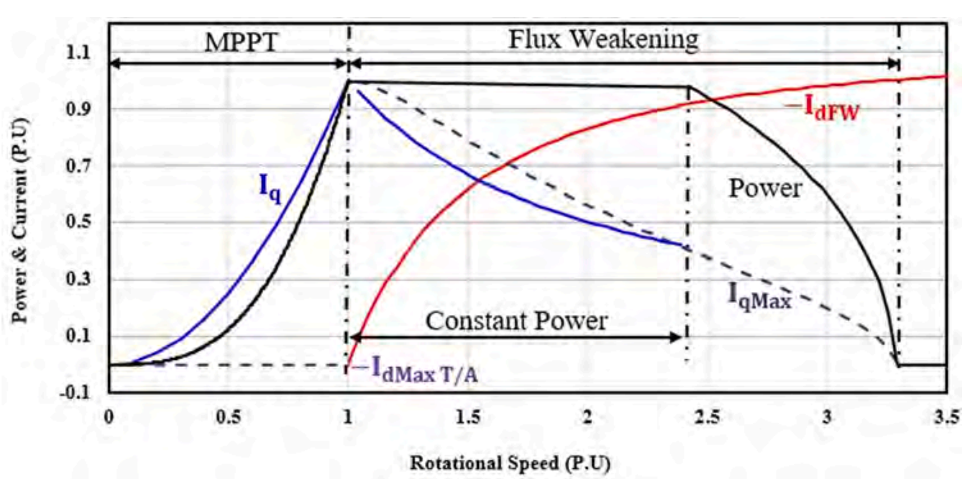

Fig. 3. Tidal turbine operating modes.

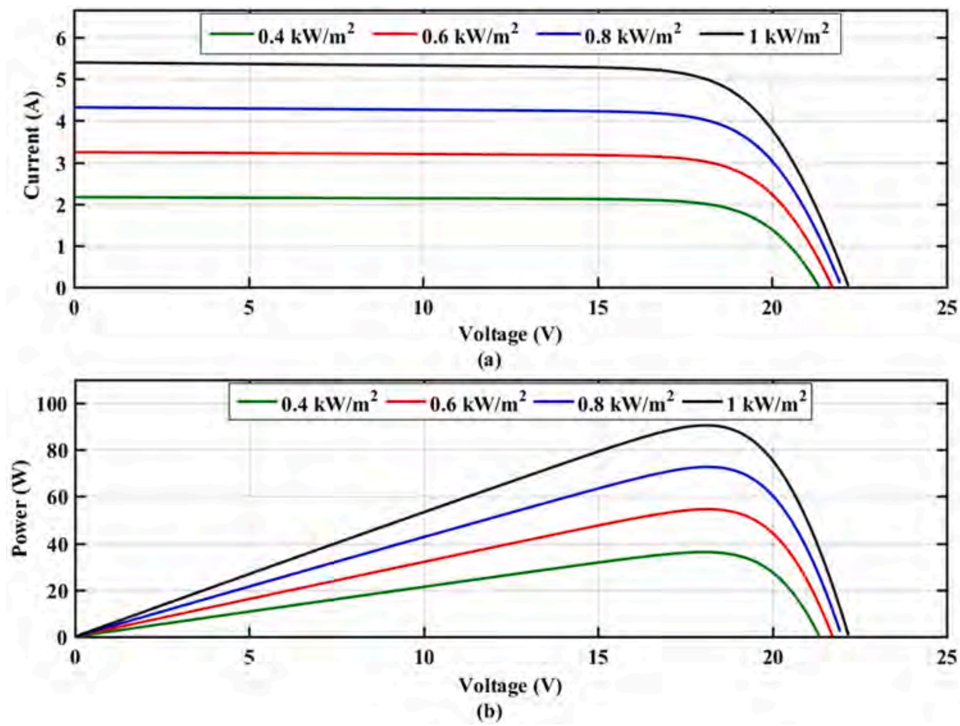

Fig. 4. (V-I) characteristic (a) and (V-P) characteristic (b) of the TE850 module at $T = 25$ °C.

occupied floor space (m^2 or ft^2), or the total power consumption (kW) [1]. For example, data centers with IT-loads varying from 10 kW to 150 kW are called small-scale whereas those with an IT-loads between 750 kW and 2.5 MW are considered to be large-scale, as presented in Table 1 [1]. In this paper, the input data were collected from the small-scale data center of the University of Technology of Belford-Montbéliard (UTBM) at 1-min intervals over one year [32]. An hourly average was carried out to reduce the number of variables as well as the computational time. The data center has a maximum IT-load of 60 kW and it can host up to 200 servers with a surface area of approximately 1506 ft^2 ($\approx$ 140 m^2) [33]. The modeling and energy management of hybrid systems is significant, especially to large-scale industries. Therefore, we scaled up the data center by a factor of 27, which requires an area of about 40,662 ft^2 ($\approx$ 3778 m^2) [34]. The maximum load of the considered data center is 1.62 MW. The power use varies between roughly 1 MW and 1.4 MW, as shown in Fig. 2.

2.2. Tidal turbine system model

The considered tidal turbine is a fixed-pitch direct-drive permanent magnet synchronous generator, with a rating of 1.5 MW. This topology has been selected to avoid the repeated outages and maintenance of the gearbox. Two power electronics converters have been integrated to assure the maximum utilization of the tidal energy besides the secure and safe interaction with the load (e.g. voltage and frequency constraints). The first converter is the machine side converter that is controlled to extract the maximum power when the turbine runs under the rated speed. When the turbine runs above the rated speed, the converter is controlled to limit the power at the rated value for protecting the system from overload and overvoltage. Fig. 3 exhibits the different operating modes of the considered turbine. The $I_{d,q}$ is the D-q axes components of the generator current, I_{qmax} is the maximum limit of the q-axis current component, I_{dFW} is the D-axis component of the flux weakening current and $I_{dMaxT/A}$ is the D-axis component of the maximum torque/amp current. The load side converter is controlled to supply an AC voltage with a fixed root mean square value of voltage and a fixed frequency on the load terminals. The detailed energetic macroscopic representation, modeling, and control of the tidal turbine, as well as the complete system parameters, have been presented in our previous work [17]. The power generated by the tidal turbine is given by (2).

$$P = \frac{1}{2}\rho A v^3 C_p \tag{2}$$

where: ρ, A, v and C_p represent the fluid density (1027 kg/m^3), the turbine swept area (πR^2), the marine current speed (m/s), and the turbine power coefficient (which is generally situated between 0.35 and 0.5 for tidal turbines), respectively [19]. C_p defines the fraction of power that can be extracted from a tidal turbine. In this study, C_p is considered to be equal to 0.45.

2.3. Solar panel model

To simulate the photovoltaic cell characteristics, equivalent circuits are used. The single diode model introduced by Alvarez-Mendoza et al. [35] is retained for its simplicity and effectiveness.

The equation connecting the current I_{PV} delivered by a PV panel (module composed of n_s cells in series and n_p in parallel) and the voltage V_{PV} is expressed by (3).

$$I_{PV} = I_{ph} - I_0\left[exp\left(\frac{V_{PV} + I_{PV}R_s}{nV_T}\right) - 1\right] - \frac{V_{PV} + I_{PV}R_s}{R_{sh}} \tag{3}$$

where: I_{ph}, I_0, n, R_s and R_{sh} stand for the photocurrent, the diode saturation current, the diode ideality factor ($n = 1.2$), the series resistance, and the shunt resistance, respectively. V_T is the diode thermal voltage and it is given by (4).

$$V_T = \frac{kT_{pv}}{q} \tag{4}$$

where: T_{pv}, k and q denote the module temperature (k), the Boltzmann constant ($k = 1.38 \times 10^{-23}$ J•k^{-1}), and the electron elementary charge ($q = 1.602 \times 10^{-19}$C), respectively.

The photovoltaic array model can be deduced from the solar model expressed above. More details can be found in [36]. In our study, we

Table 2
Electrical characteristics of the TE850 module.

Symbol	Parameter	Value
P_{MPP}	Nominal power	90 (W)
V_{MPP}	Voltage at max. power	18,1 (V)
I_{MPP}	Current at max. power	5 (A)
V_{OC}	Open circuit voltage	22,2 (V)
I_{OC}	Short circuit current	5,3 (A)

consider the TE850 module (36 cells per module) since its datasheet details are available in [36]. The (V-I) and (V-P) characteristics of this module, under different values of solar irradiance, are shown in Fig. 4, respectively. Its characteristics are summarized in Table 2. The case study is a photovoltaic array composed of 29 modules in series and 327 modules in parallel, in order to produce a maximum power of 500 kW under a DC voltage equal to 500 V and a total current equal to 1000 A.

Our goal is to deliver the highest possible power to the load by making the PV generator work at its maximum power point MPPT. The detailed energetic macroscopic representation of the PV source has been presented in [37,38].

2.4. Hydrogen energy storage system

The hydrogen system is selected due to its multiple advantages (large storage capacity (TWh), long-period charge/discharge cycle, in the range of days). The considered hydrogen energy storage system consists of an MW scale proton exchange membrane water electrolyzer (PEMWE) and fuel cell (PEMFC). The electrolyzer produces hydrogen at 30 bar to be stored on a tank of the same pressure level to be used directly by the fuel cell (no hydrogen transmission). Consequently, the proposed system does not consider a hydrogen compression system whereas a pressure regulator is required to step down the hydrogen pressure to the level of five bar as an input pressure of the fuel cell. The MW scale electrolyzer and fuel cell systems consist of six stacks of 250 kW/stack. Figs. 5 and 6 show the main characteristics of the electrolyzer and the fuel cell stacks. The electric models of the electrolyzer and fuel cell are described below.

2.4.1. Electrolyzer model

The cell voltage response of the electrolyzer is given by (5) [39-41].

$$V_{Cell} = E_{nernst} + V_{act} + V_{ohm} + V_{con} \tag{5}$$

where: E_{nernst} is the equilibrium voltage, which represents the electromotive force required for hydrogen production. It can be calculated due

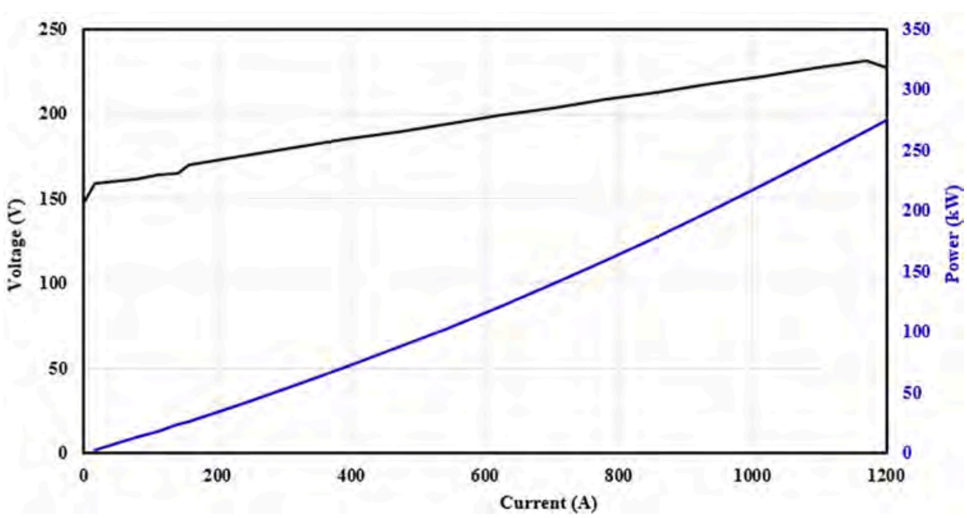

Fig. 5. Characteristics of 250 kW electrolyzer stack.

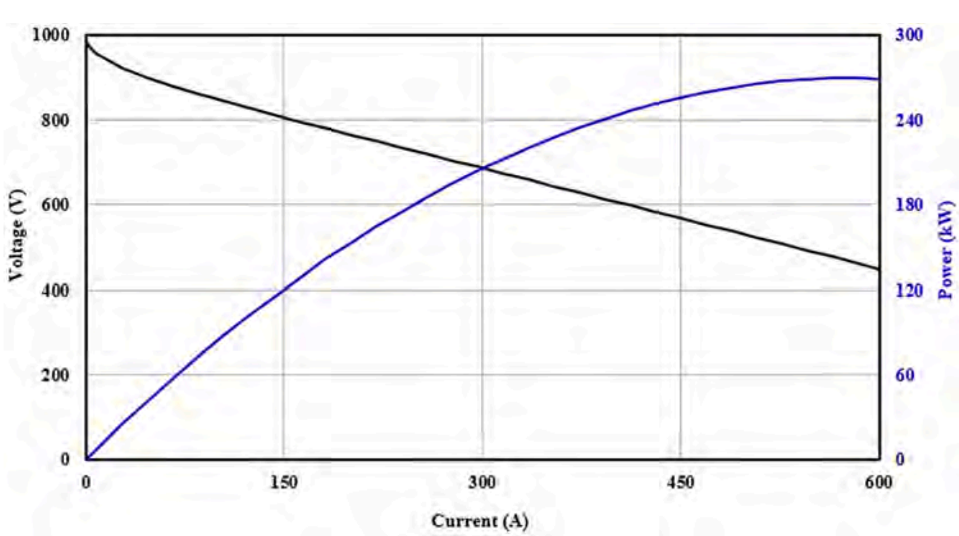

Fig. 6. Characteristics of 250 kW fuel cell stack.

to (6) and (7).

$$E_{nernst} = E_{ref} + \frac{RT}{2F} ln\left(\frac{P_{H_2} P_{O_2}^{0.5}}{P_{H_2O}}\right) \tag{6}$$

$$E_{ref} = \frac{\Delta G}{2F} = V_{std} - 0.0009\ (T - T_{std}) \tag{7}$$

where: E_{ref} is the thermodynamic voltage at standard conditions (T=25 °C and P = 1 bar), R is the universal gas constant (8.3144 J•K^{-1}•mol^{-1}), T is the stack temperature. P_{H_2}, P_{O_2} and P_{H_2O} denote the concentrations of hydrogen, oxygen, and water respectively. ΔG, V_{std} and T_{std} denote the change in molar Gibbs free energy (J•mol^{-1}), the cell voltage, and the temperature at standard conditions (V_{std}= 1.23 V).

V_{act} is the activation overvoltage, which is the required potential to start the electrochemical reaction to separate the water molecule (H_2O) into hydrogen and oxygen atoms. It can be estimated based on (8).

$$V_{act} = \frac{RT}{2F\alpha_A} sinh^{-1}\left(\frac{I_{EL}}{2A_{act}i_{0A}}\right) + \frac{RT}{2F\alpha_C} sinh^{-1}\left(\frac{I_{EL}}{2A_{act}i_{0C}}\right) \tag{8}$$

where: α_A, α_C are the anode and cathode charge transfer coefficients, respectively. i_{0A}, i_{0C} are their exchange current densities (A•cm^{-2}), I_{EL} is the electrolyzer current and A_{act} is the cell active area (cm^2).

V_{ohm} is the ohmic overvoltage, which reflects the cell voltage loss due to the cell components' resistance to the electron and proton flow. This potential is determined by considering only the electrolyte due to (9).

$$V_{ohm} = \frac{\gamma}{\sigma} i \tag{9}$$

where: γ, σ, and i represent the membrane thickness (µm), the protonic conductivity (S/cm) and the electric current density (A•cm^{-2}), respectively.

Finally, V_{con} is the concentration overvoltage, which refers to the electrical current transfer limitation due to the concentration of the gasses generated at the membrane electrode assembly (MEA). It can be expressed as follows:

$$V_{con} = \frac{RT}{4F} ln\left(\frac{C_{O_2me}}{C_{O_20}}\right) + \frac{RT}{2F} ln\left(\frac{C_{H_2me}}{C_{H_20}}\right) \tag{10}$$

where: C_{O_2me}, C_{H_2me} represent the oxygen and hydrogen concentrations at the membrane and C_{O_20}, C_{H_20} represent the oxygen and hydrogen concentrations at the reference conditions respectively.

The PEM electrolyzer stack voltage is calculated by multiplying the cell voltage V_{Cell} by the number of cells in series N_{EL} as shown in (11). The hydrogen production rate depends mainly on the operating current (I_{EL}), and it is given by (12) [26,40,41].

$$V_{EL} = N_{EL} V_{Cell} \tag{11}$$

$$\dot{n_{H_2}} = \eta_F \frac{I_{EL}}{2F} N_{EL} = \dot{n_i} N_{EL} \tag{12}$$

where $\dot{n_{H_2}}$ is the hydrogen molar flow (n•, mol/s).

2.4.2. Fuel cell model

When the microgrid suffers from an energy shortage, the hydrogen stored in the tanks is transferred to the fuel cells to convert its chemical energy into electricity. The modeling of the fuel cell is considered similar to that of the electrolyzer. However, V_{act}, V_{ohm} and V_{con} must be reviewed [40,42,43]. The output voltage of a PEMFC elementary cell (U_{Cell}) is given by (13) [42].

$$\begin{cases} U_{Cell} = E_{nernst} - U_{act} - U_{ohm} - U_{con} \\ U_{FC} = N_{FC} U_{Cell} \end{cases} \tag{13}$$

where: U_{FC} is the PEMFC stack voltage, N_{FC} is the number of cells in series. U_{act}, U_{ohm} and U_{con} denote the activation overvoltage, the ohmic overvoltage, and the concentration overvoltage, respectively. According to [44], these parameters can be expressed as follows: [42]

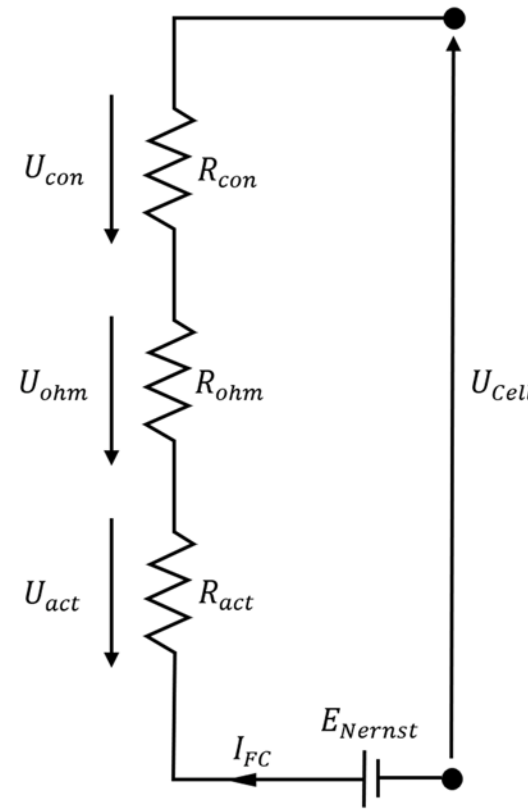

Fig. 7. Electrical model of the fuel cell.

$$\begin{cases} E_{nernst} = E_{ref} + \frac{RT}{2F}\left[ln(P_{H_2}) + \frac{1}{2} ln(P_{O_2})\right] \\ V_{act} = \frac{RT}{2F\alpha} ln\left(\frac{I_{FC}}{S_{act}J_0}\right) \\ V_{con} = -\frac{RT}{2F} ln\left(1 - \frac{I_{FC}}{S_{act}J_{max}}\right) \\ V_{ohm} = R_{ohm} I_{FC} \end{cases} \tag{14}$$

where: I_{FC} is the current of an elementary cell (A), S_{act} is the active area of the membrane, J_0 and J_{max} are the exchange current density and the maximum current density, respectively. Finally, R_{ohm} is the ohmic resistance, which is a function of the equivalent membrane impedance R_{mem} and the contact resistance R_C between the different stack layers as shown in (15).

$$R_{ohm} = R_{mem} + R_C \tag{15}$$

The electrical model representing the dynamic behavior of the fuel cells is shown in Fig. 7 [44]. The detailed energetic macroscopic representation, modeling, and control of the hydrogen energy storage system have been presented in our previous work [26,45,46]. The electrolyzer and the fuel cell systems have dynamic responses and characteristics (in our case, the ramp from zero to full load in five minutes) that must be respected for avoiding degradation and aging [26,40,45,46]. Hence, an auxiliary energy storage system must be integrated.

2.5. Battery stack

As mentioned above, the battery covers the fast dynamics of the

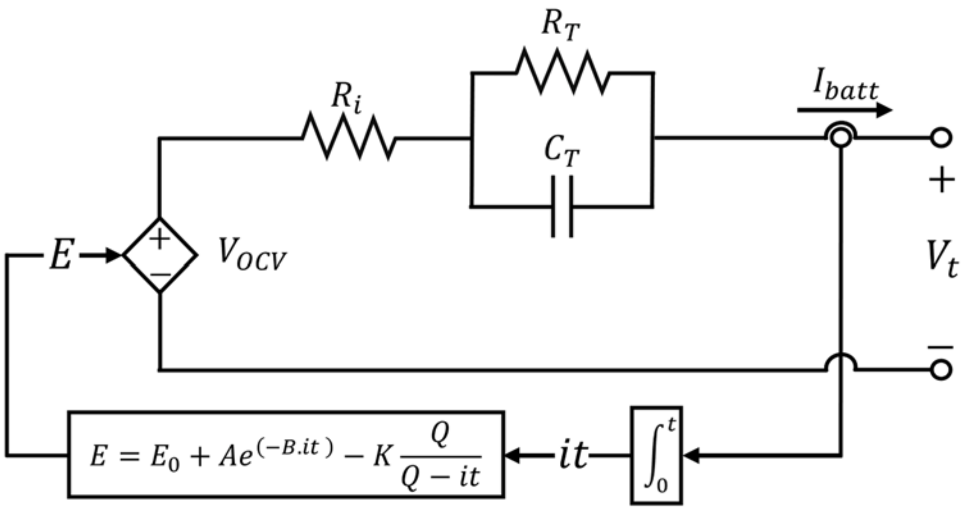

Fig. 8. $LiFePO_4$ battery cell model.

difference between the generated and the consumed powers. It has been modeled using the first-order Thevenin model, which reproduces the battery's behavior through electrical circuits. This model is composed of a voltage source V_{OCV}, a resistance R_i in series and an RC group as shown in Fig. 8 [47,48]. The Shepherd model can be expressed by (16) and (17).

$$E = E_0 - K\frac{Q}{Q - \int idt} + Ae^{\left(-B.\int idt\right)} \tag{16}$$

$$V_t = E - R_i i \tag{17}$$

where: E, E_0, V_t, i and Q are the open-circuit voltage (V), the electromotive force (V), the battery terminal voltage (V), the battery current (A), and the battery cell capacity (A•h). K, A, and B are the Shepherd model parameters and have been presented in [48].

The battery stack has been sized based on the procedure described in [49] that filters the power based on a specific time constant. The filter time constant represents the dynamic performance of the electrolyzer and the fuel cell recommended by the manufactures. The data center has a very fluctuating load profile as shown in Fig. 2. Thus, the battery stack must cover the power of 500 kW. The stack parameters have been estimated based on the 250 kW/500 kWh stack model presented in [50]. The stack has 13 parallel-connected strings of 168 cells in series (capsulated in series modules) to have a 500 kW/1000 kWh stack size. The $LiFePO_4$ battery is selected due to its dynamic response and the best advantages of power and energy densities compared to the other types [40]. The global energetic macroscopic representation of the whole system has been synthesized and presented in [26,40].

3. Energy management system

The power consumption in cloud data centers is different from that of residential loads, it is characterized by fast dynamic fluctuations which make its management a great challenge. The proposed energy management system consists of two layers; the first is the energy balance algorithm and the second is the low-level control. The energy management algorithms vary from simple rules "if-else" to complex multi-criteria optimization, including several technical-economic and environmental parameters [51]. In this paper, a filtration-based controller (FBC) has been used. The aim is to share the net power between various storage devices through a low-pass filter, as they have different dynamic characteristics as shown in Fig. 9 [49]. This method has the advantage of being simple and cost-effective. Furthermore, only a limited number of settings are required, such as the filter cut-off frequency f_c and the storage systems' charge and discharge limits [44,52]. The energy balance strategy estimates the operating points of the electrolyzer and the fuel cell (P_{EL}, P_{FC} respectively) as shown in Fig. 10. Moreover, it guarantees the safe operation of the electrolyzer, the fuel cell, and the battery. The safe operation of the electrolyzer and the fuel cell represents the dynamic response recommended by the manufacturers (as aforementioned, five minutes ramp up from zero to full load) [26,40,45,46]. Thus, a power filter with this specific time constant estimates the operating point (reference power) of the electrolyzer and the fuel cell. The simultaneous operation of the electrolyzer and the fuel cell represents the electricity-to-electricity round trip of the energy storage system. Otherwise, the stored hydrogen handling during the simultaneous operation sometimes exposes security constraints. Hence, the energy management strategy prohibits this mode of operation [40]. When the

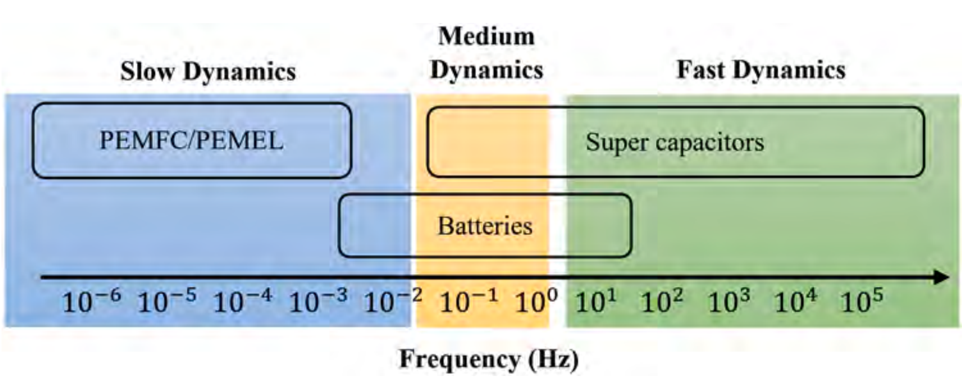

Fig. 9. Frequency diagram of some energy storage systems.

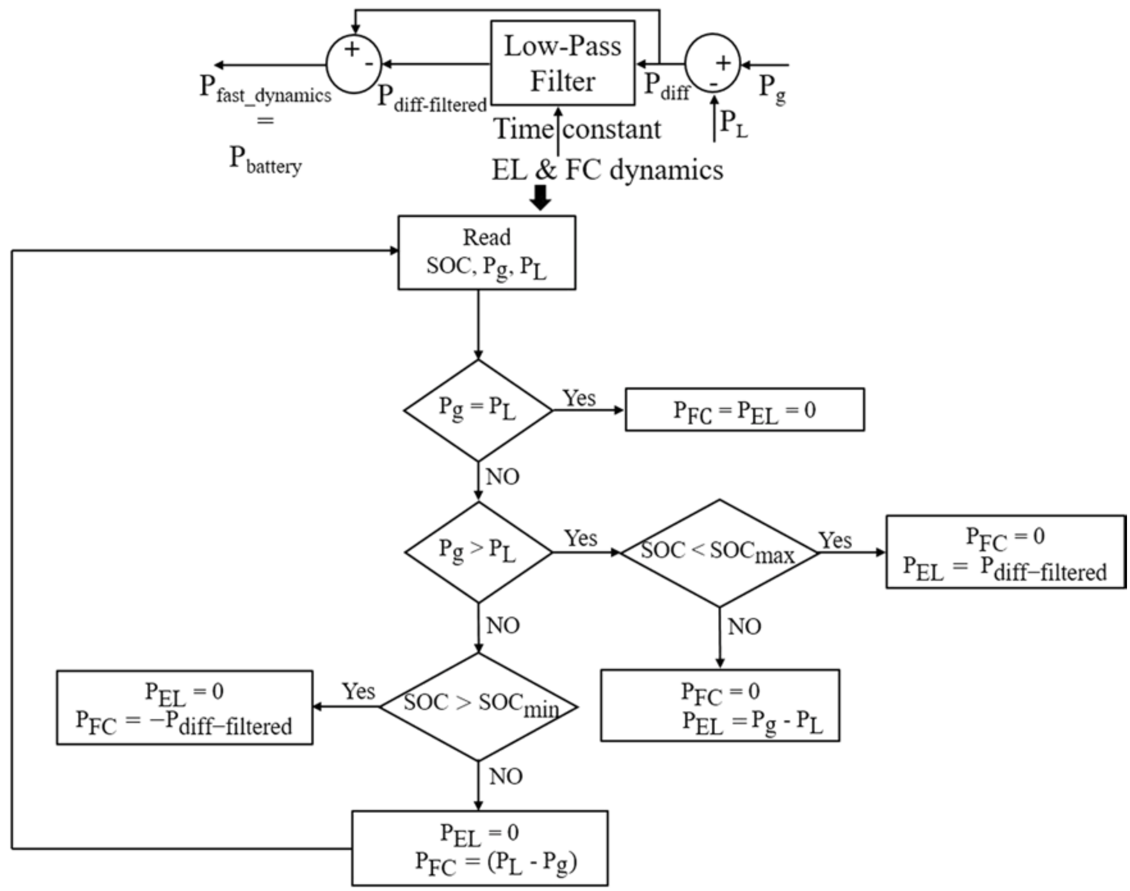

Fig. 10. Energy balance strategy.

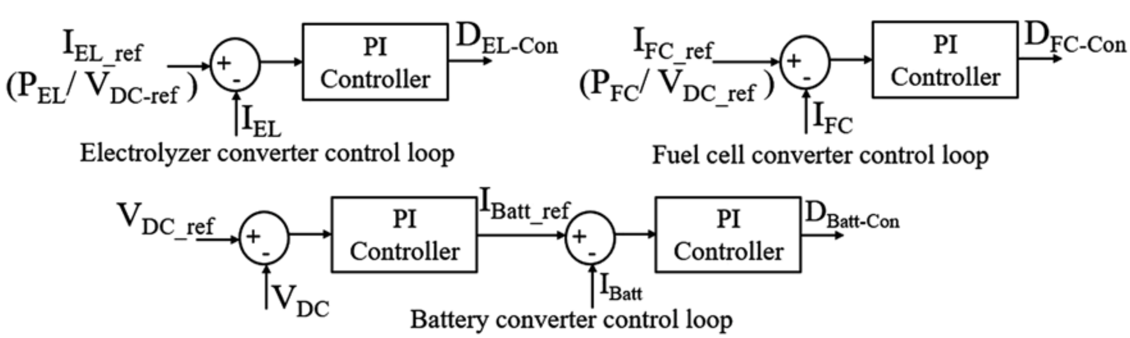

Fig. 11. Low-level control loops (Dx is the duty cycle of converter x).

generated power (Pg, tidal turbine, and photovoltaic) is higher than the consumed power (P_L), the electrolyzer is switched on to produce hydrogen. While the energy balance strategy turns the fuel cell on to compensate for the power shortage between the generation and the consumption using the stored hydrogen that has been produced during the energy welfare. The battery safe operation represents the state of charge (SoC) limits recommended by the manufacturer (depending on the battery technology and type) for avoiding overcharging and under discharging. Indeed, the recommendation is that the SoC should be between 25 and 90%. To ensure that we have sufficient energy to operate auxiliary equipment such as sensors, displays, and programmable logic controllers (PLCs), we have set the minimum limit at 40%, where the additional 15% represents the safety stock. Thus, the assumed SoC limits in the proposed case study are 90 and 40% respectively. The reference powers of the electrolyzer and the fuel cell are represented in the low-level control loops as current setpoints (I_{EL_ref}, I_{FC_ref} respectively) assuming a fixed DC link voltage (V_{DC}). Consequently, their DC-DC power electronics converters are controlled as current-controlled sources as shown in Fig. 11. The energy balance and the safe operation of the proposed microgrid, shown in Fig. 1, requires a stable DC link voltage. The battery covers the fast-dynamic component of the power difference by controlling its power electronics converter as a voltage-controlled source with a low-level dual control loop as shown in Fig. 11.

4. Case study

This work aims to implement a standalone renewable energy-based system that can provide continuous power to the green data center on a remote island. In order to evaluate the performance of the proposed energy management strategy, simulations have been conducted in Matlab/Simulink. Real data of the Alderney Race tidal current speed [53] and Cherbourg solar radiation have been used to test the system

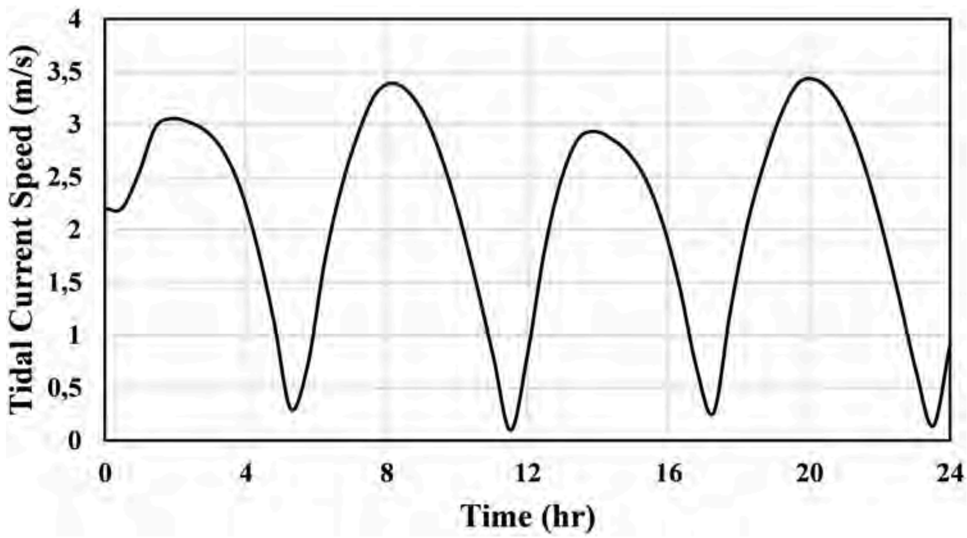

Fig. 12. Daily tidal speed profile of the Alderney Race marine site.

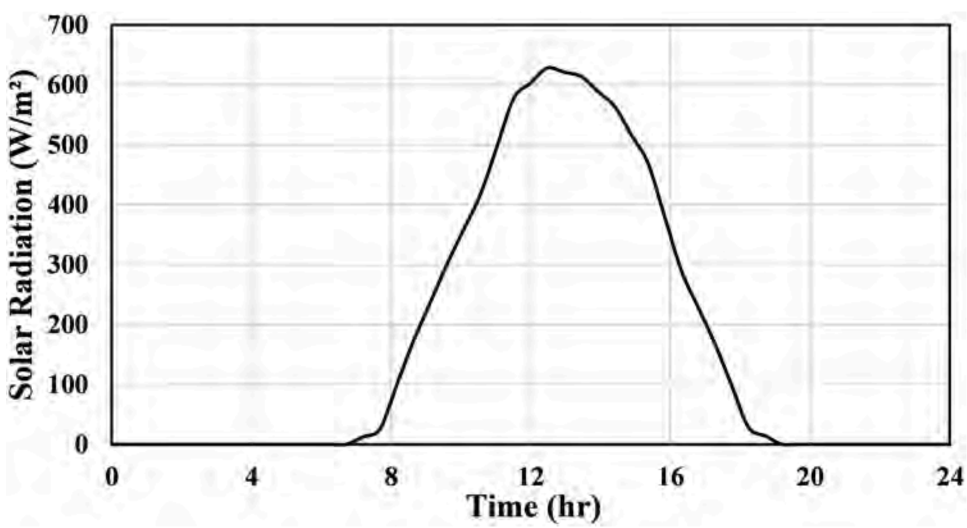

Fig. 13. Cherbourg daily solar radiation.

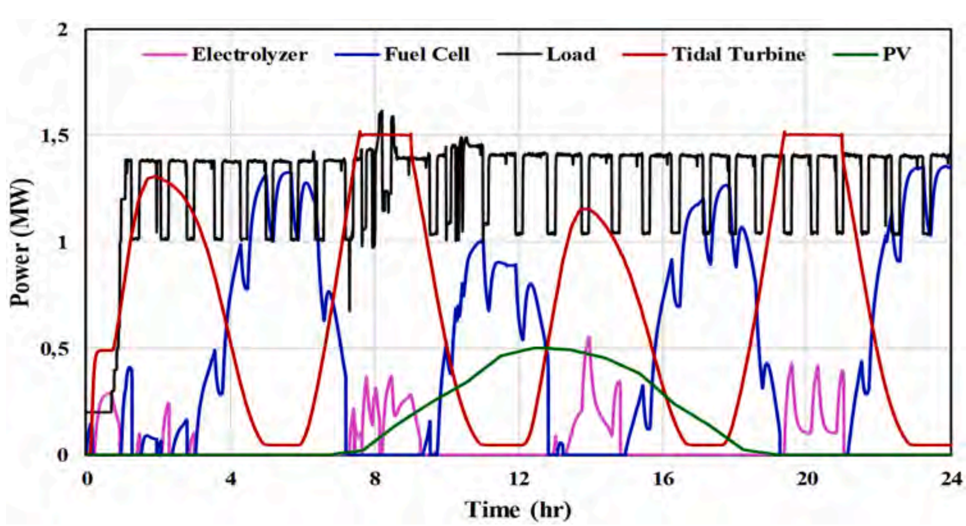

Fig. 14. Power profiles of the hybrid green data center microgrid.

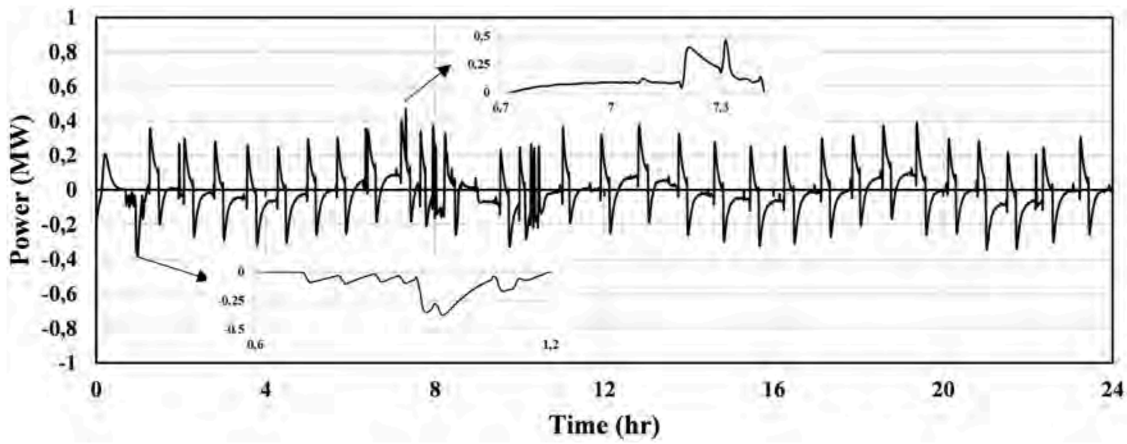

Fig. 15. Battery output power.

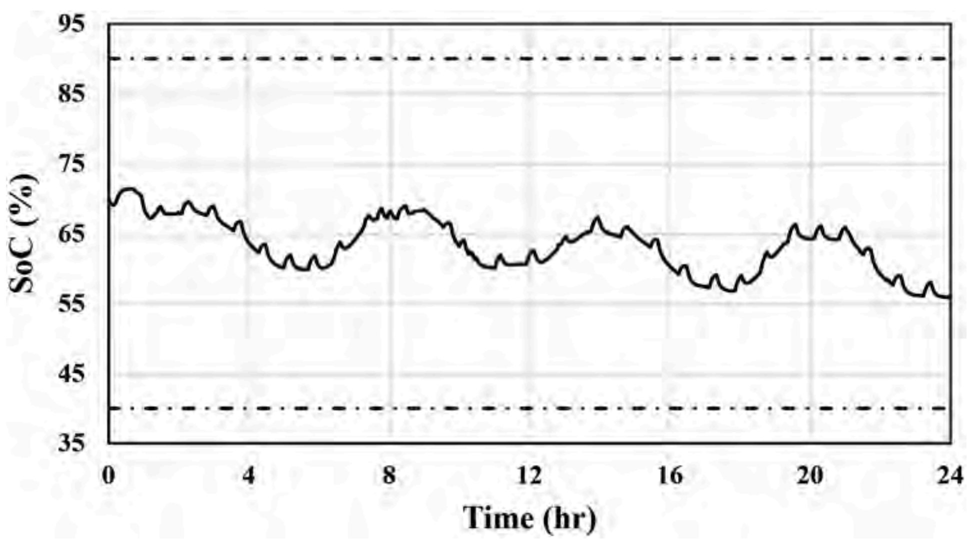

Fig. 16. State of Charge of the battery (SoC).

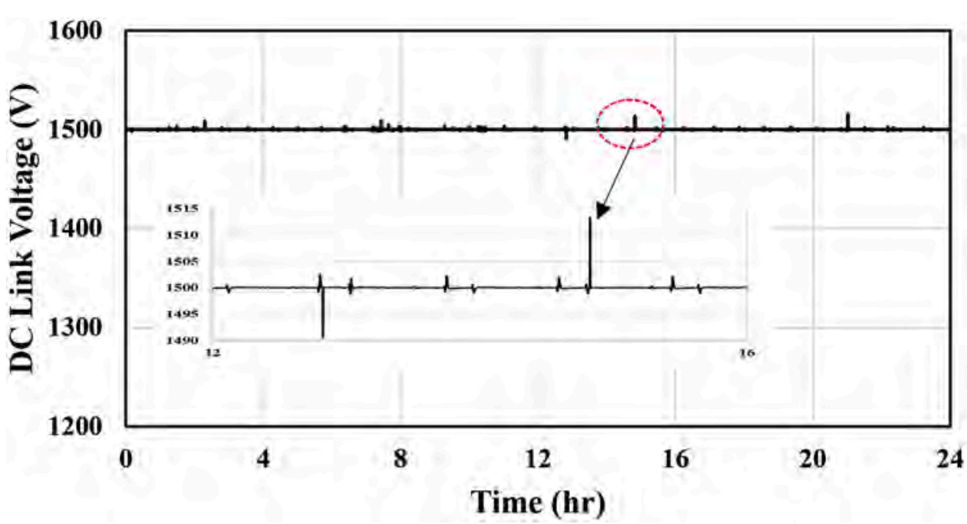

Fig. 17. DC Link voltage.

model as shown in Figs. 12 and 13, respectively. Since 15 September 2005 presents the day where the highest tide occurs according to the measurement [40], it has been selected as a case study. The studied day was sampled in 15 min to have 94 samples/day. The system power curve obtained by the management strategy is given in Figs. 14 and 15. The maximum power generated by PV panels changes according to the solar

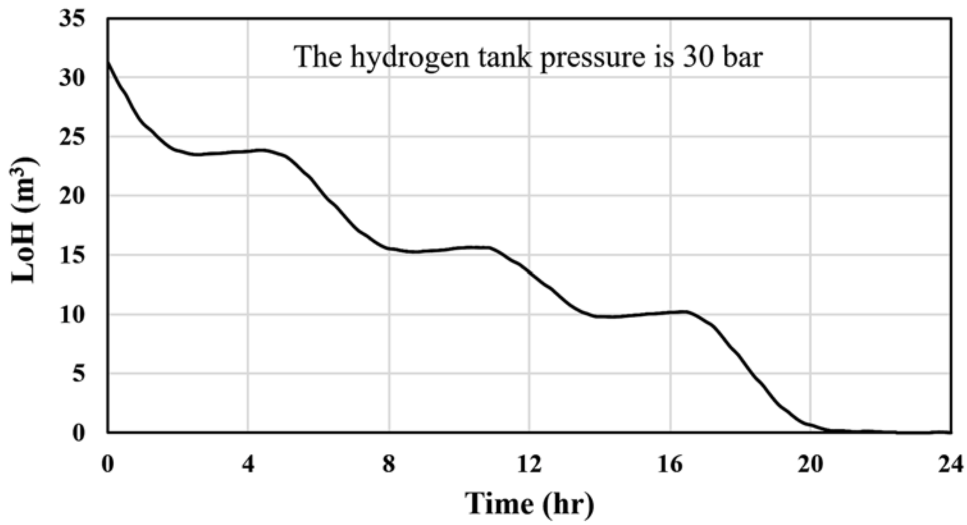

Fig. 18. Hydrogen volume at the storage tank.

radiation profile presented in Fig. 13, while the tidal turbine maximum power changes according to the tidal current speed. From the analysis of Figs. 14 and 15, it can be seen that the priority is given to the renewable sources while the storage systems are used as a backup. When the power generated exceeds the data center demand, the battery covers the system's fast dynamics if its SoC is below the maximum while the electrolyzer is used to produce hydrogen (H_2) from the excess energy up to its rated power. When the power generated is less than the data center demand, the battery smooths the fast dynamics if its SoC allows discharging while the fuel cell compensates for the unbalanced power using the hydrogen stored in the tanks. Fig. 16 shows the battery SoC, it can be observed that the proposed management strategy is designed in such a way as to keep the SoC within its defined range (within 40–90%). Besides, the SoC never reaches either its minimum or maximum limit. Fig. 17 illustrates the DC link voltage profile that is well regulated at 1500 V with a maximum variation of about 1%, due to demand and supply variation. The balance between the generation and consumption ensures this stabilization with the assistance of the battery side converter control. The pressure level of the storage tank at 100% state of charge (65 kg/day) is 30 bar. Fig. 18 shows the level of hydrogen (LoH) stored in the tanks. We can notice that the hydrogen volume decreases until the tank is empty at the end of the day, which means that the power generated by the PV panels and the tidal turbine is insufficient to supply the load for the following days (lack of sunshine or weak tidal currents). Thus, the optimal sizing of the system is mandatory to guarantee a reliable and continuous energy feeding to the load at a minimum cost for ensuring a more cost-effective installation [28,29,54-57]. Also, Power-to-Gas (P2G) is a promising technology in which excess energy is converted to gas through the electrolyzer [58].

5. Sensitivity analysis

The results of the daily profile that have been presented in the previous section are not sufficient to assess the flexibility and the effectiveness of the proposed model and the EMS. Consequently, the model with its EMS must be simulated under different operating conditions. As the computational cost of the annual profiles is very high to be afforded by the laboratory machines, a sensitivity analysis is carried out to study the impact of input data on the performance of the system under consideration, in particular the evolution of the battery state of charge and the level of hydrogen stored in the tanks.

To this end, the annual profiles of tidal speed, solar radiation, and the data center power consumption have been used. The different profiles have been clustered and regrouped into daily profiles that simulate different case studies. The solar radiation has been represented by two daily profiles; winter day (weak solar radiation) and summer day (strong solar radiation). The annual tidal speed profile has been analyzed based on the frequency of repetition (FoR) algorithm considering the studied tidal turbine characteristics of 1, 2,5, and 3,2 m/s as cut-in, rated, and cut-out speeds respectively, as shown in Fig. 3. The available data of the considered marine site (Alderney Race) has been reshaped into a matrix of 365 columns, each one has 96 values of 15 min samples as a daily profile. The reshaped matrix (365×96) has been regrouped into clusters of repeated daily speed profiles with a certain limit of tolerance as

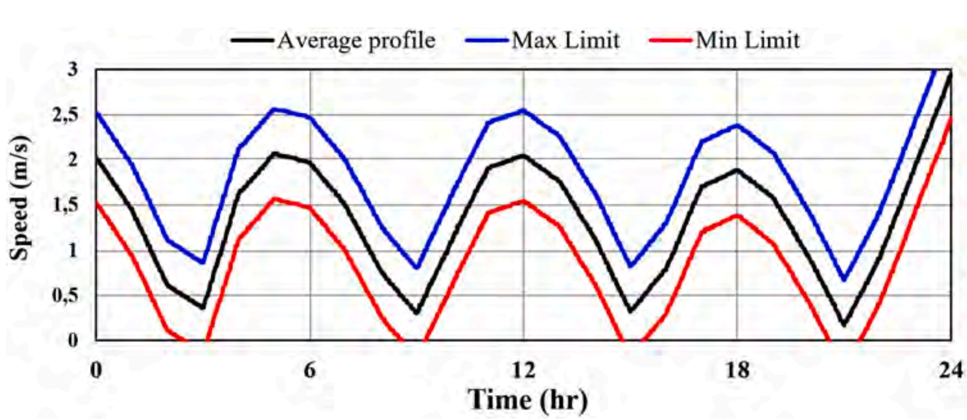

Fig. 19. Speed profile with its limit projections.

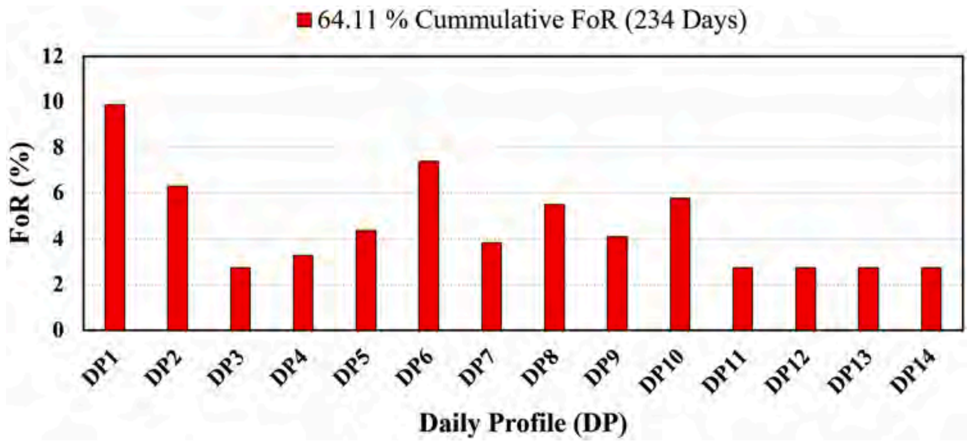

Fig. 20. Frequency of Repetition (FoR) of each speed profile.

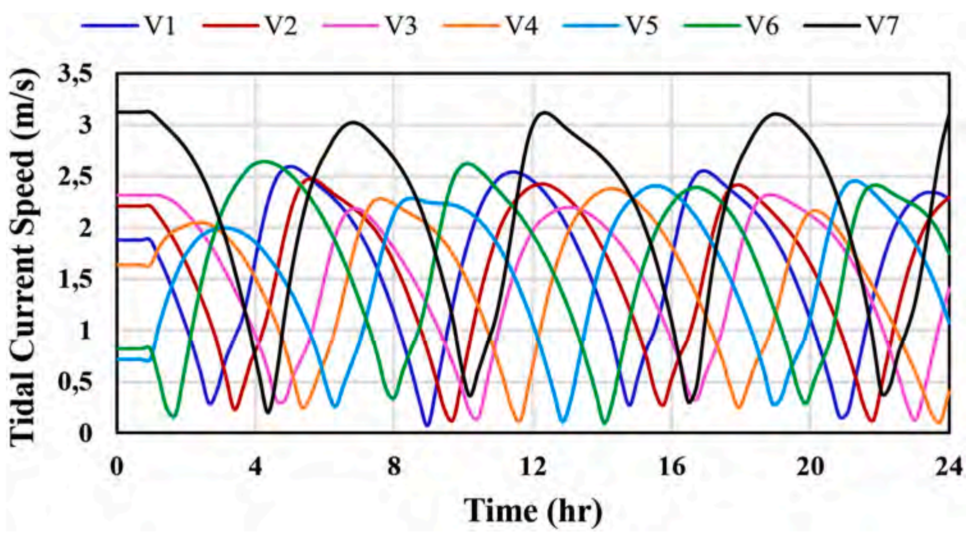

Fig. 21. Speed profiles in the Winter case study.

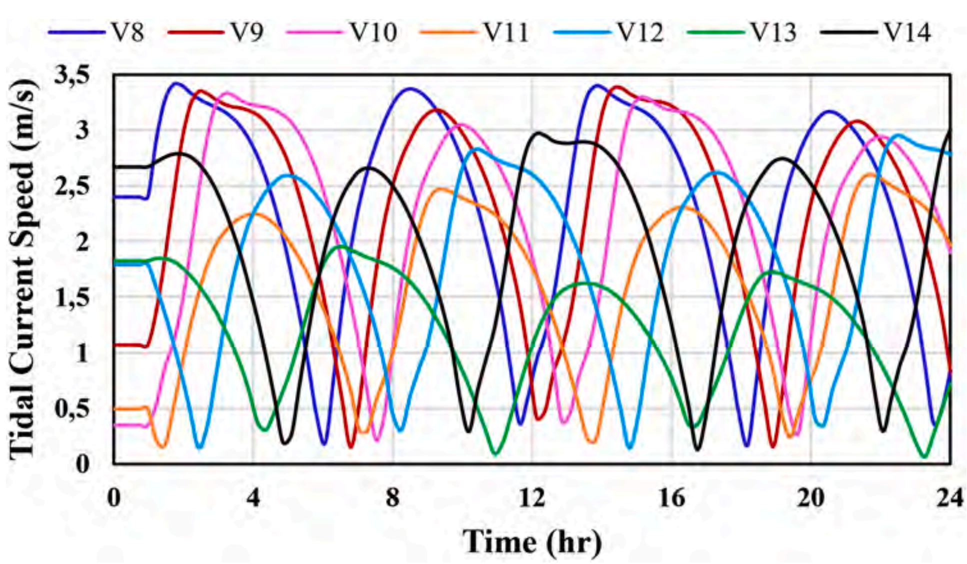

Fig. 22. Speed profiles in the summer case study.

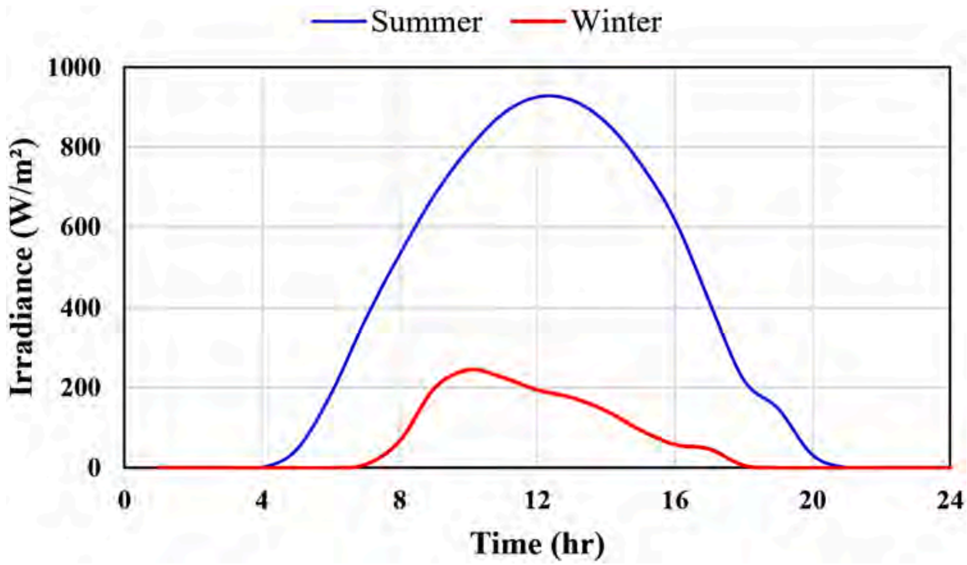

Fig. 23. Winter and Summer solar radiation case studies.

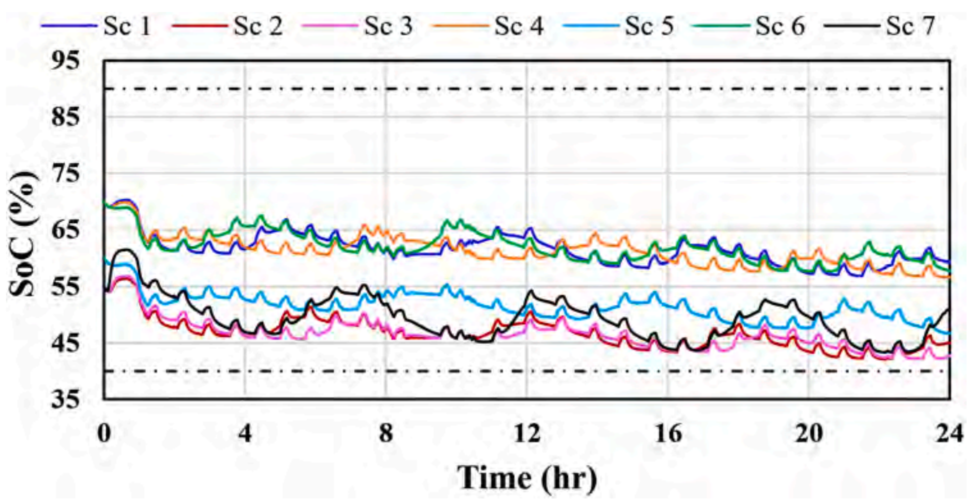

Fig. 24. Battery SoC in the Winter case study.

shown in Fig. 19. The selected speed tolerance is 1 m/s as a compromise between the computation cost and the data clustering accuracy. The speed matrix has been debugged by an M-File /MATLAB code of the proposed FoR clustering algorithm. The code provides 66 daily profiles representing the annual data. The most frequently repeated daily profiles ($\geq$ 10 times) have been selected to simulate the proposed model. Thus, 14 daily profiles with the highest FoR (representing 234 days of the considered annual data), as shown in Fig. 20, have been regrouped into the two case studies; 7 profiles with the winter case study and 7 profiles with the summer case study (Figs. 21–23). The proposed model (with its EMS) has been launched 14 times simulating the two case studies that provide the results presented in the following paragraphs.

Figs. 24 and 25 show the battery state of charge for the 14 scenarios in the winter and summer case studies, respectively, where "*Sc*" stands for scenario. The solar radiation and the speed of tidal current have a direct effect on the battery SoC. During the winter, the SoC ranges between 40 and 60% for scenarios 2,3,5, and 7, while it does not even reach 55% for the other ones. This is explained by the difference in the tides' average speed, under the same solar radiation profile. As for the summer, the average SoC of the battery remains between 60 and 75%. Since the city of Cherbourg is known for its rainy climate and low sunlight in winter, the battery discharges more energy during this period than in summer. However, in both cases, the SoC remains within the two upper and lower limits previously specified (between 40 and 90%). This shows that the proposed power management strategy is efficient, protecting the battery from premature aging and keeping a 15% back-up all day long.

Figs. 26 and 27 illustrate the amount of hydrogen stored in tanks in the considered 14 scenarios. In most cases, the hybrid system requires more hydrogen in the winter than in the summer to fulfill the data center's needs throughout the day. A significant difference in the amount of hydrogen required at the beginning of each day in the summer season is observed for the same reason mentioned above (disparity in the tidal currents average speed). Indeed, the mean velocity for the first three scenarios is 2,31, 2,25 and 2,15 m/s respectively, while for the last four scenarios it is 1,59, 1,84, 1,21 and 1,98 m/s. Over the 7 winter scenarios, the average amount of hydrogen needed is 59.7 m^3, almost twice the amount consumed in the reference case study with the highest tide. As for the consumption during summer, it is 41.46 m^3, i.e. 133% of the reference case.

Since the considered profiles represent 234 days of the annual data available, the energy management strategy adopted can give us an idea

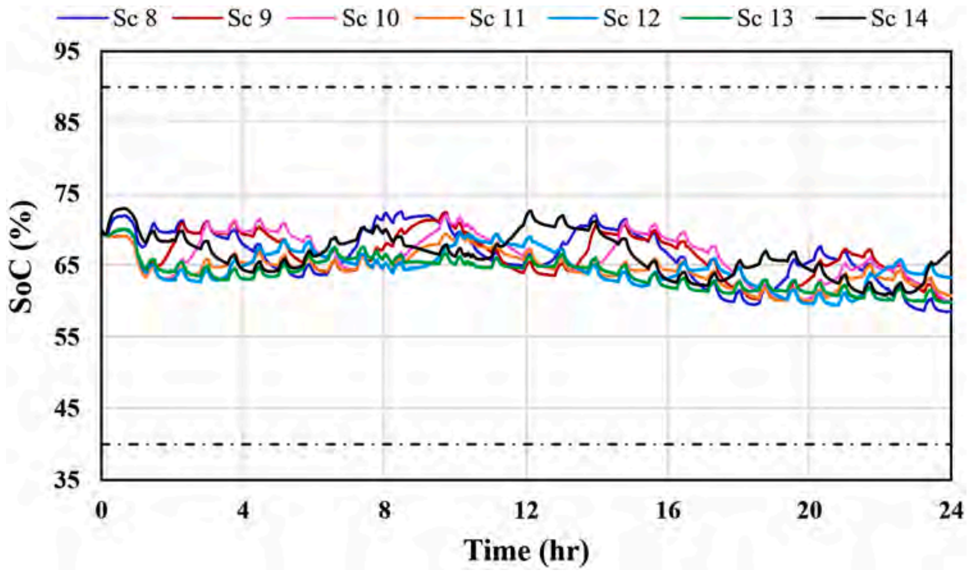

Fig. 25. Battery SoC in the Summer case study.

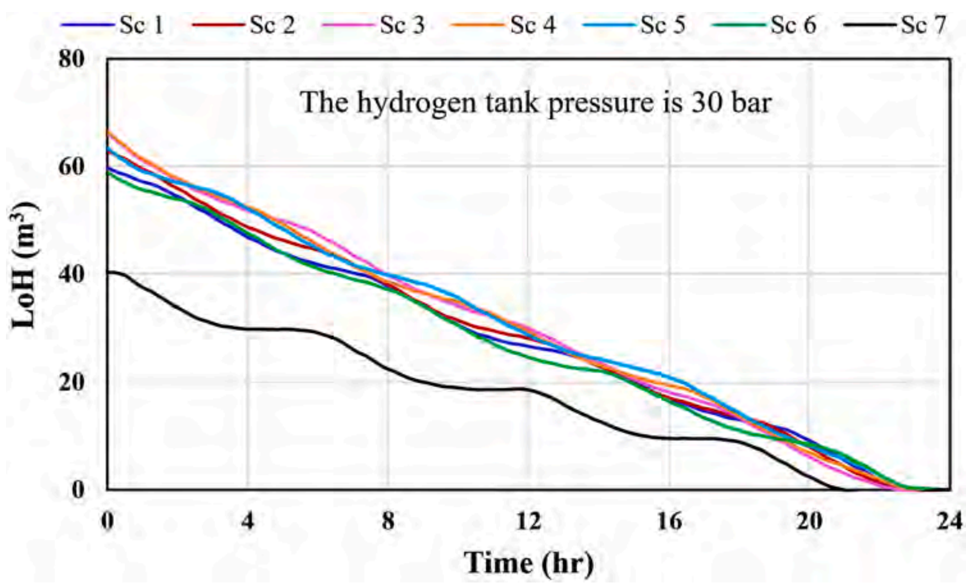

Fig. 26. Level of Hydrogen in the Winter case study.

of the hydrogen volume required by the data center, at a defined pressure (30 bar in our case), to ensure its operation throughout the year. This information can be used as an input for the sizing optimization program to increase the convergence speed and reduce computing time. Moreover, this EMS can be applied to any data center type with different solar radiation and tidal current speed profiles.

6. Conclusion

In this paper, using energetic macroscopic representation, the modeling and the energy management of a hybrid isolated Tidal/PV system to feed an MW scale data center have been developed. Due to the available energy sources' intermittent nature, hydrogen and battery have been selected as a combined energy storage system. The first is responsible for the system's slow dynamics whereas the second is responsible for smoothing the system's fast dynamics. The model has been implemented in Matlab/Simulink to evaluate its performance under different operating conditions. It can be used for different applications, such as grid-connected, standalone, etc. The main objective of this model is to determine the behavior of a data center powered by renewable energies, particularly, its performance and the storage type that is suitable for it.

Through the analysis of the results, it is found that the battery SoC was maintained within its defined range. However, the hydrogen volume stored in the tanks was not sufficient to supply the load due to the considered daily profiles as a case study. Many requirements are necessary to have a safe operation of the system. Firstly, the storage system must operate within its defined limits. Secondly, the system must comply with the operating recommendations defined by the manufacturer of each component. Finally, sustainable energy feeding must be guaranteed. For this purpose and as a future work proposal, an optimization of the different subsystems sizing as well as the energy management system must be carried out, considering the cost and the lifespan. Moreover, the surplus energy can be sold either in P2G mode or as electricity to the main grid. In addition, and based on the data center dynamics, the possibility of sharing power between batteries and

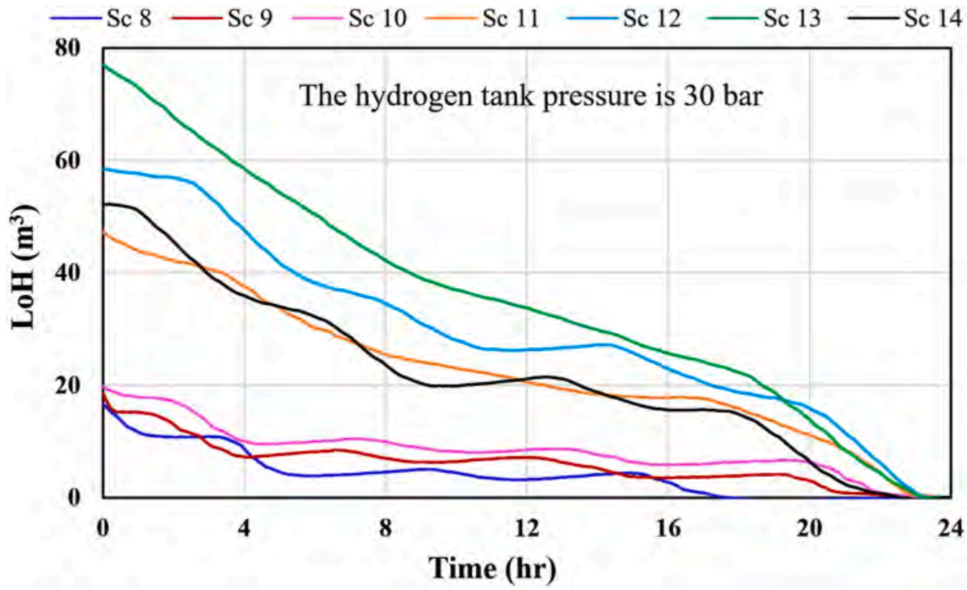

Fig. 27. Level of Hydrogen in the Summer case study.

another storage system such as supercapacitors for improving the system performance might be studied.

This study affirms that supplying data centers with renewable resources is feasible provided that the system is properly sized and it is worthwhile to take advantage of the energy that can be extracted from tidal currents and solar irradiation.

CRediT author contribution statement

Nouhaila Lazaar: Conceptualization, Methodology, Software, Writing-Original Draft, Writing-Review & Editing. **Mahmoud Barakat:** Conceptualization, Methodology, Software, Writing-Original Draft, Writing-Review & Editing. **Morad Hafiane:** Writing-Review & Editing. **Jalal Sabor:** Writing - Review & Editing, Supervision, Project administration. **Hamid Gualous:** Writing - Review & Editing, Supervision, Project administration.

Declaration of Competing Interest

The authors declare that they have no known competing financial interests or personal relationships that could have appeared to influence the work reported in this paper.

Acknowledgments

This work was supported by contracts and projects of LUSAC Laboratory, which funded the Ph.D. thesis of the first author.

References

[1] C. Koronen, Demand-Response Potential of Large-Scale Data Centers in Europe 2030," M.S. thesis, Dept. Technol. Soc., Lund Univ., Lund, Sweden, 2018.
[2] L. Grange, G. Da Costa, P. Stolf, Green IT scheduling for data center powered with renewable energy, Fut. Gen. Comp. Syst. 86 (2018) 99120, https://doi.org/10.1016/j.future.2018.03.049. Sept.
[3] A. Andrae, T. Edler, On global electricity usage of communication technology: trends to 2030, Chall 6 (1) (2015), 117157, https://doi.org/10.3390/challe6010117. Apr.
[4] I. Goiri, W. Katsak, K. Le, T.D. Nguyen, R. Bianchini, Parasol and GreenSwitch: managing datacenters powered by renewable energy, in: Proc. ASPLOS, Houston, Texas, USA, 2013, p. 13, https://doi.org/10.1145/2451116.2451123.
[5] Y. Guo, Y. Gong, Y. Fang, P.P. Khargonekar, X. Geng, Energy and network aware workload management for sustainable data centers with thermal storage, IEEE Trans. Parallel Distrib. Syst. 25 (8) (2014) 2030–2042, https://doi.org/10.1109/TPDS.2013.278. Aug.
[6] "Sustainability in numbers," Facebook Sustainability, Accessed on: apr. 20, 2020. [Online]. Available: https://sustainability.fb.com/sustainability-in-numbers/.
[7] "Project Natick phase 2," Microsoft, Accessed on: apr. 20, 2020. [Online]. Available: https://natick.research.microsoft.com/.
[8] M. Ghamkhari, H. Mohsenian-Rad, Energy and performance management of green data centers: a profit maximization approach, IEEE Trans. Sma. Grid 4 (2) (2013), 10171025, https://doi.org/10.1109/TSG.2013.2237929. June.
[9] K. Kim, F. Yang, V.M. Zavala, A.A. Chien, Data centers as dispatchable loads to harness stranded power, IEEE Trans. Sustain. Energy 8 (1) (2017), 208218, https://doi.org/10.1109/TSTE.2016.2593607. Jan.
[10] P. Funck, "Are Islanded Microgrids suitable for mission critical facilities?," Mission Critical, Feb. 02, 2016. Accessed on: jul. 06, 2020. [Online]. Available: https://www.missioncriticalmagazine.com/articles/88136-are-islanded-microgrids-suitable-for-mission-critical-facilities.
[11] M.H. Nawaz, M.U. Khan, A. Zahra, M. Ali, R. Wazir, K. Ullah, Optimal Economic Analysis of Hybrid Off Grid (Standalone) Energy system for provincial capitals of pakistan: a comparative study based on simulated results using real-time data, in: Proc. PGSRET, Islamabad, Pakistan, 2018, pp. 1–6, https://doi.org/10.1109/PGSRET.2018.8685991.
[12] L. Mellouk, M. Ghazi, A. Aaroud, M. Boulmalf, D. Benhaddou, K. Zine-Dine, Design and energy management optimization for hybrid renewable energy system-case study: Laayoune region, Ren. Ene. 139 (2019), 621634, https://doi.org/10.1016/j.renene.2019.02.066. Aug.
[13] J. Ahmed, Z. Salam, A modified P&O maximum power point tracking method with reduced steady-state oscillation and improved tracking efficiency, IEEE Trans. Sustain. Energy 7 (4) (2016), 15061515, https://doi.org/10.1109/TSTE.2016.2568043. Oct.
[14] A.G. Shaik, O.P. Mahela, Power quality assessment and event detection in hybrid power system, Electr. Power Syst. Res. 161 (2018) 26–44, https://doi.org/10.1016/j.epsr.2018.03.026. Aug.
[15] M.A. Hossain, H.R. Pota, S. Squartini, F. Zaman, K.M. Muttaqi, Energy management of community microgrids considering degradation cost of battery, J. Ene. Sto. 22 (2019), 257269, https://doi.org/10.1016/j.est.2018.12.021. Apr.
[16] S.E.B. Elghali, M.E.H. Benbouzid, J.F. Charpentier, Marine tidal current electric power generation technology: state of the art and current status, in: Proc. IEEE Int. Conf. Electric Machines & Drives, Antalya, Turkey, 2007, 14071412, https://doi.org/10.1109/IEMDC.2007.383635.
[17] M.R. Barakat, B. Tala-Ighil, H. Chaoui, H. Gualous, Y. Slamani, D. Hissel, Energetic macroscopic representation of a marine current turbine system with loss minimization control, IEEE Trans. Sustain. Energy 9 (1) (2018), 106117, https://doi.org/10.1109/TSTE.2017.2716926. Jan.
[18] M. Liu, W. Li, R. Billinton, C. Wang, J. Yu, Modeling tidal current speed using a Wakeby distribution, Electr. Power Syst. Res. 127 (2015) 240–248, https://doi.org/10.1016/j.epsr.2015.06.014. Oct.
[19] S.E. Ben Elghali, M.E.H. Benbouzid, J.-.F. Charpentier, Modelling and control of a marine current turbine-driven doubly fed induction generator, IET Renew. Power Gener. 4 (1) (2010) 1–11, https://doi.org/10.1049/iet-rpg.2008.0118. Jan.
[20] O.A.L. Brutto, M.R. Barakat, S.S. Guillou, J. Thiebot, H. Gualous, Influence of the wake effect on electrical dynamics of commercial tidal farms: application to the Alderney Race (France), IEEE Trans. Sustain. Energy 9 (1) (2018), 321332, https://doi.org/10.1109/TSTE.2017.2731839. Jan.
[21] S. Hazim, A.E. Ouatouati, M.T. Janan, A. Ghennioui, Marine currents energy resource characterization for Morocco, Energy Procedia 157 (2019) 1037–1049, https://doi.org/10.1016/j.egypro.2018.11.271. Jan.

[22] K. Mergoul, B. Laarabi, A. Barhdadi, Solar water pumping applications in Morocco: state of the art, in: Proc. IRSEC, Rabat, Morocco, 2019, p. 16, https://doi.org/10.1109/IRSEC.2018.8703015.
[23] P. Sinha, W. Hayes, B. Littmann, L. Ngan, R. Znaidi, Environmental variables affecting solar photovoltaic energy generation in Morocco, in: Proc. IRSEC, Ouarzazate, Morocco, 2015, pp. 230–234, https://doi.org/10.1109/IRSEC.2014.7059897.
[24] M. Petrucci, Noor Midelt I: Morocco builds an outstanding hybrid solar power plant [Noor Midelt I: le Maroc construit une centrale solaire hybride hors norme], Masen (2019). Jul. 23 Accessed on: Apr. 20, 2020. [Online]. Available: http://www.masen.ma/.
[25] H.E.Z. Farag, A. Al-Obaidi, H. Khani, N. El-Taweel, E.F. El-Saadany, H.H. Zeineldin, Optimal operation management of distributed and centralized electrolysis-based hydrogen generation and storage systems, Electr. Power Syst. Res. 187 (2020), 106476, https://doi.org/10.1016/j.epsr.2020.106476. Oct.
[26] M.R. Barakat, B. Tala-Ighil, H. Gualous, D. Hissel, Modeling of a hybrid marine current-hydrogen active power generation system, Int. J. Hydrogen Energy 44 (19) (2019), 96219635, https://doi.org/10.1016/j.ijhydene.2018.10.020. Apr.
[27] J. Morel, S. Obara, K. Sato, D. Mikawa, H. Watanabe, T. Tanaka, Contribution of a hydrogen storage-transportation system to the frequency regulation of a microgrid, in: Proc. ICRERA, Palermo, Italy, 2015, 510514, https://doi.org/10.1109/ICRERA.2015.7418465.
[28] N. Lazaar, E. Fakhri, M. Barakat, H. Gualous, J. Sabor, Optimal sizing of marine current energy based hybrid Microgrid, Renew. Energy Power Qual. J. 18 (2020) 515–521, https://doi.org/10.24084/repqj18.417. Jun.
[29] N. Lazaar, E. Fakhri, M. Barakat, J. Sabor, H. Gualous, A genetic algorithm based optimal sizing strategy for PV/Battery/Hydrogen hybrid system,", in: Artificial Intelligence and Industrial Applications, vol. 144, T. Masrour, I. El Hassani, and A. Cherrafi, Eds. Cham: springer International Publishing, 2021, pp. 247–259.
[30] Z. Wang, F. Liu, Y. Chen, S.H. Low, S. Mei, Unified distributed control of stand-alone DC microgrids, IEEE Trans. Smart Grid 10 (1) (2019) 1013–1024, https://doi.org/10.1109/TSG.2017.2757498. Jan.
[31] H. Cheung, S. Wang, C. Zhuang, J. Gu, A simplified power consumption model of information technology (IT) equipment in data centers for energy system real-time dynamic simulation, Appl. Energy. 222 (2018), 329342, https://doi.org/10.1016/j.apenergy.2018.03.138. Jul.
[32] R. Roche, "Datacenter data," Accessed on: apr. 20, 2020. [Online]. Available: https://www.robinroche.com/wordpress/data-and-links/.
[33] Nadège, The new UTBM data center will be powerful, ecological and educational [Le nouveau datacenter de l'UTBM sera puissant, écologique et pédagogique], Détours (2014). Dec. 17Accessed on: Apr. 20, 2020. [Online]. Available: http://detours.utbm.fr/2014/12/17/datacenter-pedagogie-puissance/.
[34] N. Pham, Data centers: jobs and opportunities in communities nationwide, SSRN Electron. J. (2017) 20, https://doi.org/10.2139/ssrn.2998644. May.
[35] F. Alvarez-Mendoza, C. Angeles-Camacho, P. Bacher, H. Madsen, Semi-dispatchable generation with wind-photovoltaic-fuel cell hybrid system to mitigate frequency disturbance, Electr. Power Syst. Res. 165 (2018) 60–67, https://doi.org/10.1016/j.epsr.2018.08.021. Dec.
[36] K.S. Agbli, "Energy Flows Modelling of a PEM electrolyser- Photovoltaic Generator-PEM Fuel Cell Coupling Dedicated to Stationary Applications [Modélisation multiphysique des flux énergétiques d'un couplage photovoltaïque-electrolyseur PEM–pile à combustible PEM en vue d'une application stationnaire]," Ph.D. dissertation, Dept. Ene., Cocody-Abidjan Univ., Abidjan, Côte d'Ivoire, 2018.
[37] K.S. Agbli, D. Hissel, M.-.C. Péra, I. Doumbia, EMR modelling of a hydrogen-based electrical energy storage, The Eur. Phys. J. Appl. Phys. 54 (2) (2011) 11, https://doi.org/10.1051/epjap/2010100272. May.
[38] A. Badis, M.N. Mansouri, M.H. Boujmil, A genetic algorithm optimized MPPT controller for a PV system with DC-DC boost converter, in: Proc. ICEMIS, Monastir, Tunisia, 2018, p. 16, https://doi.org/10.1109/ICEMIS.2017.8273010.
[39] M. Espinosa-López, et al., Modelling and experimental validation of a 46kW PEM high pressure water electrolyzer, Ren. Energy 119 (2018), 160173, https://doi.org/10.1016/j.renene.2017.11.081. Apr.
[40] M. Barakat, "Development of Models for Integrating Renewables and Energy Storage Components in Smart Grid Applications," Ph.D. dissertation, Dept. Elect. Eng., Caen Normandy Univ., Cherbourg, France, 2018.
[41] P. Fragiacomo, M. Genovese, Modeling and energy demand analysis of a scalable green hydrogen production system, Int. J. Hydrogen Energy 44 (57) (2019), 3023730255, https://doi.org/10.1016/j.ijhydene.2019.09.186. Nov.
[42] L. Kong, J. Yu, G. Cai, Modeling, control and simulation of a photovoltaic /hydrogen/supercapacitor hybrid power generation system for grid-connected applications, Int. J. Hydrogen Energy 44 (46) (2019), 2512925144, https://doi.org/10.1016/j.ijhydene.2019.05.097. Sept.
[43] F. Alshehri, V.G. Suárez, J.L. Rueda Torres, A. Perilla, M.A.M.M. van der Meijden, Modelling and evaluation of PEM hydrogen technologies for frequency ancillary services in future multi-energy sustainable power systems, Heliyon 5 (4) (2019) e01396, https://doi.org/10.1016/j.heliyon.2019.e01396. Apr.
[44] C. Mahjoubi, "Multi-Physics Modeling and Energy Management of a Residential micro-grid [Modélisation multi-physique et gestion d'énergie d'un micro-réseau résidentiel autonome],", Dept. Elect. Eng., Nantes Univ., Nantes, France, 2018. Ph.D. dissertation.
[45] M. Barakat, B. Tala-Ighil, H. Chaoui, H. Gualous, D. Hissel, Energy management of a hybrid tidal turbine-hydrogen micro-grid: losses minimization strategy, Fuel Cells (2020), https://doi.org/10.1002/fuce.201900082. May.
[46] M.R. Barakat, B. Tala-Ighil, H. Gualous, D. Hissel, JADE based multi-agent decentralized energy management system of a hybrid marine-hydrogen Power Generation System, in: Proc. ELECTRIMACS, Salerno, Italy, 2019.
[47] D.N.T. How, M.A. Hannan, M.S. Hossain Lipu, P.J. Ker, State of charge estimation for Lithium-Ion batteries using model-based and data-driven methods: a review, IEEE Access 7 (2019), 136116136136, https://doi.org/10.1109/ACCESS.2019.2942213.
[48] K. Bae, S. Choi, J. Kim, C. Won, Y. Jung, LiFePO4 dynamic battery modeling for battery simulator, in: Proc. ICIT, Busan, South Korea, 2014, 354358, https://doi.org/10.1109/ICIT.2014.6894892.
[49] K.S. Agbli, M. Barakat, H. Gualous, D. Hissel, Large scale tidal hydrogen production for fuel cell based EVs,", in: presented at ELECTRIMACS 2017, Toulouse, France, Jul. 4-6, 2017.
[50] P. Kubiak, Z. Cen, C.M. López, I. Belharouak, Calendar aging of a 250kW/500kWh Li-ion battery deployed for the grid storage application, J. Pow. Sour. 372 (2017) 1623, https://doi.org/10.1016/j.jpowsour.2017.10.063. Dec.
[51] C. Bordons, F. Garcia-Torres, M.A. Ridao, Model Predictive Control of Microgrids, Springer Nature Switzerland AG, Cham, Switzerland, 2020. ISBN 978-3-030-24569-6.
[52] S. Hajiaghasi, A. Salemnia, M. Hamzeh, Hybrid energy storage system for microgrids applications: a review, J. Energy Storage 21 (2019) 543–570, https://doi.org/10.1016/j.est.2018.12.017. Feb.
[53] J. Thiébot, P. Bailly du Bois, S. Guillou, Numerical modeling of the effect of tidal stream turbines on the hydrodynamics and the sediment transport – Application to the Alderney Race (Raz Blanchard), France, Renew. Energy 75 (2015) 356–365, https://doi.org/10.1016/j.renene.2014.10.021. Mar.
[54] Lin Xu, Xinbo Ruan, Chengxiong Mao, Buhan Zhang, Yi Luo, An improved optimal sizing method for wind-solar-battery hybrid power system, IEEE Trans. Sustain. Energy 4 (3) (2013), 774785, https://doi.org/10.1109/TSTE.2012.2228509. Jul.
[55] T. Mesbahi, F. Khenfri, N. Rizoug, P. Bartholomeus, P.L. Moigne, Combined optimal sizing and control of Li-Ion battery/supercapacitor embedded power supply using hybrid particle swarm–Nelder–Mead algorithm, IEEE Trans. Sustain. Energy 8 (1) (2017) 5973, https://doi.org/10.1109/TSTE.2016.2582927. Jan.
[56] Y. Ding, Q. Xu, Y. Huang, Optimal sizing of user-side energy storage considering demand management and scheduling cycle, Electr. Power Syst. Res. 184 (2020), 106284, https://doi.org/10.1016/j.epsr.2020.106284. Jul.
[57] M. Farrokhifar, F.H. Aghdam, A. Alahyari, A. Monavari, A. Safari, Optimal energy management and sizing of renewable energy and battery systems in residential sectors via a stochastic MILP model, Electr. Power Syst. Res. 187 (2020), 106483, https://doi.org/10.1016/j.epsr.2020.106483. Oct.
[58] M. Berger, D. Radu, R. Fonteneau, T. Deschuyteneer, G. Detienne, D. Ernst, The role of power-to-gas and carbon capture technologies in cross-sector decarbonisation strategies, Electr. Power Syst. Res. 180 (2020), 106039, https://doi.org/10.1016/j.epsr.2019.106039. Mar.